

# ARMFlow: AutoRegressive MeanFlow for Online 3D Human Reaction Generation

Zichen Geng<sup>1</sup>, Zeeshan Hayder<sup>2</sup>, Wei Liu<sup>1</sup>, Hesheng Wang<sup>3\*</sup>, Ajmal Saeed Mian<sup>1</sup>

<sup>1</sup>The University of Western Australia, Perth, WA, Australia

<sup>2</sup>Commonwealth Scientific and Industrial Research Organisation (CSIRO), Canberra, ACT, Australia

<sup>3</sup>Shanghai Jiao Tong University, Shanghai, China

zen.geng@research.uwa.edu.au  
 {wei.liu, ajmal.mian}@uwa.edu.au  
 zeeshan.hayder@data61.csiro.au  
 wanghesheng@sjtu.edu.cn

## Abstract

3D human reaction generation faces three main challenges: (1) high motion fidelity, (2) real-time inference, and (3) autoregressive adaptability for online scenarios. Existing methods fail to meet all three simultaneously. We propose ARMFlow, a MeanFlow-based autoregressive framework that models temporal dependencies between actor and reactor motions. It consists of a causal context encoder and an MLP-based velocity predictor. We introduce Bootstrap Contextual Encoding (BSCE) in training, encoding generated history instead of the ground-truth ones, to alleviate error accumulation in autoregressive generation. We further introduce the offline variant ReMFlow, achieving state-of-the-art performance with the fastest inference among offline methods. Our ARMFlow addresses key limitations of online settings by: (1) enhancing semantic alignment via a global contextual encoder; (2) achieving high accuracy and low latency in a single-step inference; and (3) reducing accumulated errors through BSCE. Our single-step online generation surpasses existing online methods on InterHuman and InterX by over 40% in FID, while matching offline state-of-the-art performance despite using only partial sequence conditions. Code is available in the supplementary.

## 1. Introduction

Recent advances in generative modeling have led to remarkable progress in 3D human motion generation, covering a wide spectrum of tasks and methodologies. These include text-guided motion synthesis [3, 10, 11, 30, 34, 37, 45–47], human–object interaction [5, 8, 17, 28, 43], scene-conditioned motion generation, and multi-person interaction modeling. Among these, one particularly distinctive

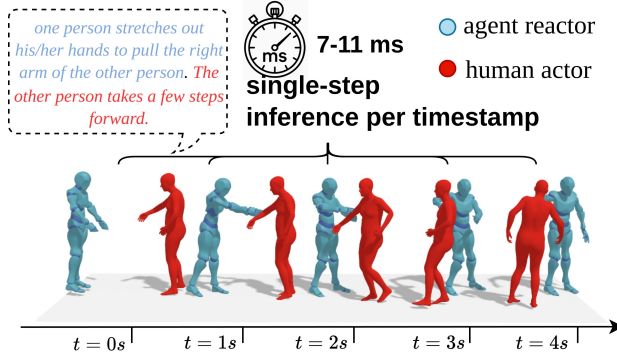


Figure 1. Our method only processes a single inference in each real-time step for online reaction generation, compared to the SOTA methods ReGenNet (35–78 ms), and CAMDM (45 ms). The text description is from the InterX [41] dataset.

task is human reaction generation, which focuses on producing reactive human behaviors in response to other agents or stimuli. This task holds immediate practical potential in human–robot interaction, augmented, and virtual realities.

Unlike *offline motion generation* tasks that rely on pre-defined conditions and tolerate second-level latency, *3D human reaction generation* demands real-time responsiveness, where the input condition evolves continuously and unpredictably. In such settings, even minimal computational delays can compromise the system’s reactivity and realism. This imposes stricter requirements on the generation framework, introducing three key challenges: (1) achieving high inference efficiency to meet real-time constraints; (2) maintaining high-fidelity motion quality to ensure natural and expressive reactions; and (3) capturing long-term contextual dependencies to preserve semantic consistency and generate accurate, context-aware motions.

Existing approaches have made attempts to address these challenges, yet fundamental limitations remain. To enable

\*Corresponding author

online generation, autoregressive architectures are essential, as they inherently model temporal dependencies between past and future motions. Methods such as CAMDM [2] and HumanX [16] adopt autoregressive diffusion models, where a fixed-length historical window serves as the conditioning context for current denoising steps. However, this design faces two key limitations: (1) the fixed context window hinders scalability and leads to inevitable information loss, causing semantic drift over long sequences; and (2) although accelerated samplers such as DDIM have been adopted, they still require multiple denoising steps (typically  $\geq 8$ ), which is computationally demanding, especially under fine-grained temporal resolutions.

To address the aforementioned three challenges and two key limitations of prior works, we propose ARMFlow, a scalable autoregressive architecture capable of generating high-fidelity human reactions in a *single-step inference*. Our method is built upon the recently proposed MeanFlow [7] paradigm, which enables one-step generation as opposed to multi-step denoising or iterative integration required by diffusion or traditional flow-based models. This is the first work that leverages MeanFlow for human motion generation, demonstrating the fastest inference speed while maintaining superior motion realism compared to existing approaches. To overcome the limitations of fixed-length contextual windows commonly used in prior autoregressive models, we introduce a causal context encoder that encodes the entire motion history with causal masking. This design prevents the loss of information beyond the context window and preserves global temporal semantics, ensuring coherent long-term motion generation.

Furthermore, we observe that training the model with only clean past motions makes it overly sensitive to noise during autoregressive generation, as it never learns to handle imperfect or accumulated prediction errors in its historical context. To mitigate this issue, we propose Bootstrap Context Encoding (BSCE), where the model uses predicted motion histories—rather than ground-truth ones during training to construct the contextual conditions for the flow velocity predictor. As training progresses, the predicted motion sequences gradually approximate real trajectories, leading to an adaptive curriculum that naturally reduces context noise over time. We further increase the number of bootstrap iterations throughout training, effectively introducing controlled noise and enhancing model robustness against accumulated prediction errors. This mechanism accelerates convergence and improves autoregressive stability. Benefiting from MeanFlow’s single-step inference, BSCE can efficiently generate augmented history samples without costly iterative denoising, resulting in significantly improved training efficiency. Together, these components form a self-consistent and efficient autoregressive generation framework based on MeanFlow dynamics.

Beyond the online setting, we further design a general offline variant, Reaction MeanFlow (ReMFlow), which serves as a versatile baseline for offline motion generation. Compared with existing state-of-the-art (SOTA) offline models, ReMFlow achieves superior generation quality and the fastest inference speed on both InterHuman and InterX benchmarks. More importantly, our online model ARMFlow not only achieves SOTA performance in real-time settings, notably over 40% on FID, but also performs on par with, and in some cases surpasses, many offline models that have access to the entire conditioning sequence simultaneously. In summary, our contributions are threefold:

1. We propose ARMFlow, a flexible and scalable method consisting of a context encoder with an MLP velocity predictor that captures global semantic alignment in an autoregressive manner.
2. We extend the MeanFlow paradigm to the domain of 3D reaction generation, introducing a unified framework for both online (ARMFlow) and offline (ReMFlow) settings that achieves single-step, high-fidelity motion synthesis with real-time performance.
3. We propose a Bootstrap Context Encoding (BSCE) mechanism that effectively mitigates error accumulation in autoregressive generation, speeds up the model’s convergence, and enhances inference robustness.

## 2. Related Works

**Reaction Generation:** 3D human motion generation is currently an active area of research, encompassing tasks such as Text-to-Motion [3, 10, 11, 29, 30, 34, 37, 45, 47], Human-Object Interaction [5, 8, 17, 28, 38, 43], to Human-Human Interaction [15, 20, 31, 39] generation. However, Action-Reaction Generation is still an understudied area. Tab. 1 lists current SOTA models for reaction generation.

Table 1. Current reaction generation models. AR: Autoregression.

| Model          | Online | Real-time | Long-context | AR |
|----------------|--------|-----------|--------------|----|
| InterMask [15] | ✗      | ✗         | ✓            | ✗  |
| InterGen [20]  | ✗      | ✗         | ✓            | ✗  |
| MARRS [40]     | ✗      | ✓         | ✓            | ✗  |
| CAMDM [2]      | ✓      | ✓         | ✗            | ✓  |
| ReGenNet [42]  | ✓      | ✓         | ✗            | ✗  |
| HumanX [16]    | ✓      | ✓         | ✗            | ✓  |
| Ours           | ✓      | ✓         | ✓            | ✓  |

Chopin et al. [4] first proposed Interformer, a Transformer-based [36] reaction synthesis model, but due to the use of traditional autoencoders to predict current actions, its prediction accuracy is less than ideal. Xu et al. [42] introduced the first online Transformer-decoder-based diffusion model, aiming to achieve both efficiency and accuracy in diffusion via DDIM [32]. Although this method performs online generation, it inherently lacks autoregression (AR) (i.e., generating the current action based on previ-

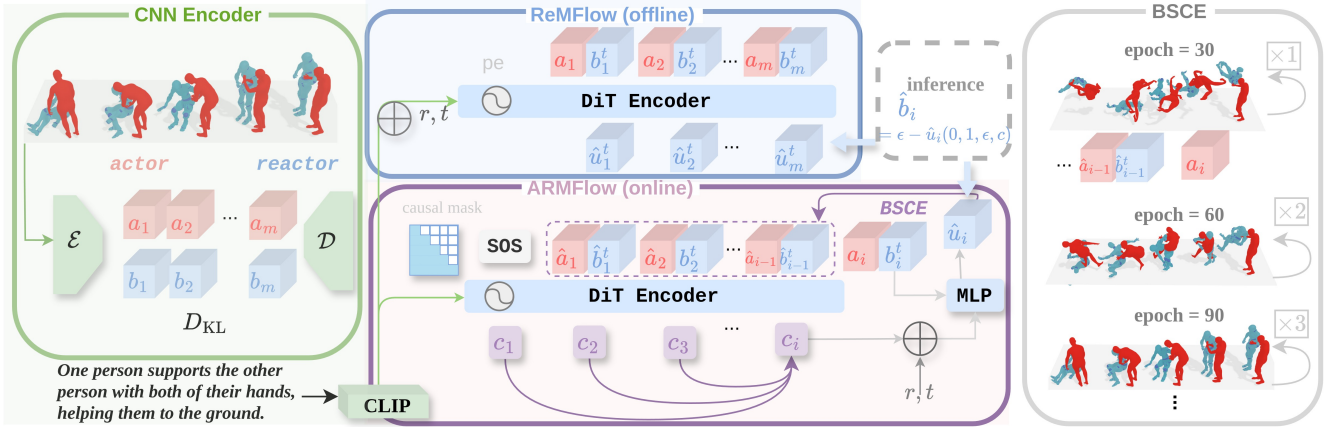


Figure 2. Overview of the proposed architecture for online and offline reaction generation. The framework consists of a CNN-based encoder to learn a compact latent space for the actor and the reactor. The ReMFlow is for offline generation based on the DiT architecture, and ARMFlow is the autoregressive online model consisting of a DiT context encoder and an MLP velocity predictor. A BSCE strategy is employed during online training progressively to reduce accumulated error in the autoregression.

ously generated content), leading to temporal inconsistency. Ji et al. [16] addressed the autoregressive online generation issue by conditioning on a fixed window of previous context to guide the generation of the next timestep’s action. However, a fixed-window design imposes significant scalability constraints: it cannot be adapted to finer temporal resolutions, and approaches such as [2] are unable to perform inference from scratch without any prior context. Moreover, when processing long sequences, the limited receptive field fails to capture distant dependencies, leading to cumulative error and lack of global contextual understanding.

**Autoregressive generative models** have been extensively explored, particularly for image generation. Some approaches tokenize continuous representations into discrete token spaces in an LLM-style manner [1, 35, 44, 45], while others adopt diffusion-based methods [12, 14, 18, 19] in an autoregressive fashion. Another line of research employs autoregressive flow-based architectures [9, 33]. Although autoregressive models are capable of capturing strong dependencies within data distributions, a core challenge lies in mitigating error accumulation that naturally occurs during sequential inference. T2M-GPT [45] addresses this issue by introducing random token corruption during training, forcing the model to correct corrupted past contexts. Subsequently, Tian et al. [35] proposed a hierarchical data representation to alleviate cumulative errors. However, these techniques are not directly applicable to conventional autoregressive models—especially diffusion-based architectures with fixed contextual windows [12, 14, 18]. To overcome this limitation, Li et al. [19] proposed a general framework combining an autoregressive context encoder with a lightweight MLP denoiser, leveraging MAE-style random masking [13] to reduce error propagation along the au-

toregressive direction. Nevertheless, such random masking schemes are less suitable for specially ordered or real-time generation tasks, where temporal consistency is essential. As a result, enhancing the robustness of real-time autoregressive models remains unsolved.

### 3. Preliminary

MeanFlow [7] is a recently proposed generative paradigm that aims to produce high-fidelity samples with only a single inference step. Unlike traditional Flow Matching (FM) [21, 23] approaches, which learn the instantaneous velocity field by estimating the continuous trajectory between data and noise distributions through numerous integration steps, MeanFlow instead models the mean velocity over the entire trajectory. Specifically, instead of computing the instantaneous flow  $\mathbf{v}(x, t)$  at each time step, MeanFlow evaluates the average transport velocity between any two points  $r$  and  $t$  in the field. This simplification allows the model to generate samples by a single-step integration of the mean field from  $r = 0$  (noise) to  $t = 1$  (data), substantially reducing inference time while maintaining strong generative quality. Our method builds upon MeanFlow, which predicts an average velocity field that bridges a Gaussian noise distribution and the target motion distribution, enabling efficient offline reaction generation with controllable conditioning and single-step inference. Given an instantaneous velocity field  $v(z_\tau, \tau)$ , the average velocity between timesteps  $r$  and  $t$  is defined as:

$$u(z_t, r, t) = \frac{1}{t - r} \int_r^t v(z_\tau, \tau) d\tau, \quad (1)$$

which captures the cumulative dynamics over the interval  $[r, t]$  and provides a smooth approximation of trajectory evolution. Differentiating both sides using the Leibniz rule

yields the training objective:

$$\mathcal{L}(\theta) = \mathbb{E} \|u_\theta(z_t, r, t) - \text{sg}(u_{\text{tgt}})\|_2^2, \quad (2)$$

$$u_{\text{tgt}} = v(z_t, t) - (t - r)(v(z_t, t) \partial_z u_\theta + \partial_t u_\theta), \quad (3)$$

where  $\text{sg}(\cdot)$  denotes the stop-gradient operator to stabilize optimization. The Jacobian–vector products (JVPs) for  $\partial_z u_\theta$  and  $\partial_t u_\theta$  are computed via automatic differentiation, avoiding explicit Jacobian construction and reducing memory overhead while maintaining accurate gradient signals. Unlike conventional flow-based methods that uniformly sample timestep pairs, we adopt a *biased sampling strategy* where a proportion of pairs satisfy  $r = t$ . This allocation strengthens the learning of the instantaneous velocity  $v(z_t, t)$ , improves convergence, and enhances fidelity for high-frequency motion components, which are critical for reactive behaviors. A key advantage of MeanFlow is single-step inference, eliminating iterative refinement:

$$\hat{z}_0 = \epsilon - u_\theta(\epsilon, 0, 1), \quad \epsilon \sim \mathcal{N}(0, I), \quad (4)$$

which drastically reduces inference cost compared to multi-step diffusion or flow-based models, making it suitable for large-scale generation.

To improve controllability without additional inference overhead, Geng et al. [7] incorporate *classifier-free guidance* (CFG) during training rather than post-hoc blending by constructing a Ground-Truth Field. The modified objective becomes:

$$\mathcal{L}(\theta) = \mathbb{E} \|u_\theta^{\text{cfg}}(z_t, r, t | c) - \text{sg}(u_{\text{tgt}})\|_2^2, \quad (5)$$

$$u_{\text{tgt}} = \tilde{v}_t - (t - r)(\tilde{v}_t \partial_z u_\theta^{\text{cfg}} + \partial_t u_\theta^{\text{cfg}}), \quad (6)$$

$$\tilde{v}_t = \omega v_t + (1 - \omega)u_\theta^{\text{cfg}}(z_t, t, t), \quad (7)$$

where  $c$  denotes the conditioning signal, and  $\omega > 1$  controls the blend between conditional and unconditional velocity fields. Training with CFG not only enhances the model’s robustness and fidelity, but also reduces the extra calculation in inference for unconditional output.

## 4. Method

Given a text description  $text$  and an actor motion sequence  $x_a \in \mathbb{R}^{T,D}$ , where  $T$  denotes the number of frames and  $D$  the pose dimension, our goal is to synthesize a realistic reactor motion  $x_b \in \mathbb{R}^{T,D}$ . The generation can occur in two modes: *sequential (online)*, where frames are predicted progressively, or *offline*, where the entire sequence is generated in a single pass. To achieve this, we first compress actor and reactor motions into a shared latent space using the CNN-VAE described in Section 4.1, which benefits both offline and online reaction generation. Building on this representation, we introduce **ReMFlow** (Section 4.2) for offline generation and **ARMFlow** (Section 4.3) for online generation,

both leveraging the MeanFlow framework and a DiT-based backbone [27]. Finally, we propose the *Bootstrap Context Encoding* (BCSE), which is inherently suited for ARMFlow and mitigates error accumulation during autoregression.

### 4.1. CNN-VAE for Motion Compression

To enhance generation efficiency and model robustness, we adopt a 1D-CNN VAE following the T2M-GPT [45] architecture to compress actor–reactor motion sequences  $\mathbf{x} = \{\mathbf{x}_a, \mathbf{x}_b\}$  into two temporal latent representations  $\{\mathbf{a}, \mathbf{b}\}$ . This compression serves two purposes: (1) It reduces the dimensionality of motion data for efficient transmission and computation, and (2) provides a structured latent space that facilitates autoregressive modeling.

Unlike canonicalized actor motion, reactor motion is highly dynamic and lacks a standardized representation, making discrete quantization prone to severe accuracy degradation. To address this, we employ continuous latent tokens with KL-divergence regularization instead of discrete codes. This design embeds motion into a compact yet expressive latent space, accelerating convergence and improving reconstruction fidelity. Furthermore, the causal nature of 1D-CNN ensures that temporal dependencies are preserved, enabling efficient disentanglement of latent tokens in online generation. This property significantly enhances flexibility when handling sequential contexts.

The VAE objective is defined as:

$$\mathcal{L}_{\text{VAE}} = \mathbb{E}_{q(z|x)} [\log p(x|z)] - \text{KL}(q(z|x) \| p(z)), \quad (8)$$

where  $q(z|x)$  is the encoder distribution,  $p(x|z)$  is the decoder likelihood, and  $p(z)$  is the Gaussian prior. To facilitate high-fidelity VAE reconstruction, we employ inverse kinematic (IK) loss for explicit joint position and velocity loss for motion smoothness.

### 4.2. ReMFlow for Offline Reaction Generation

We implement **ReMFlow** for offline generation using a DiT-based encoder with multimodal conditioning. Text prompts are encoded via a CLIP text encoder [24] and fused with timestep embeddings to form a global condition vector, which is injected into DiT through adaptive layer normalization (AdaLN) to modulate intermediate activations. Actor tokens  $a_i$  are concatenated with interpolated reactor tokens  $b_i^t$ , encoded from a CNN-based VAE to capture local appearance and dynamics of the reactor. These tokens are aligned along the last dimension, summed with positional encodings, and processed by DiT to predict average velocities  $\mathbf{u} = \{u_i\}_{i=1}^m$  over tokenized spatiotemporal patches. To enable unconditional learning and support CFG, a proportion of text and actor tokens are replaced with null tokens  $\emptyset$  during training, which regularizes the model and stabilizes optimization under varying conditioning strengths.

This design allows ReMFlow to jointly model actor dynamics and reactor responses under flexible conditioning while maintaining computational efficiency. Compared to iterative diffusion models, our approach achieves significant speedup and scalability due to single-step inference and average-velocity prediction, making it practical for large-scale offline reaction generation tasks without sacrificing fidelity or semantic alignment.

### 4.3. ARMFlow for Online Generation

**ARMFlow** overcomes the limitations of fixed-window architectures by enabling encoding from scratch and retaining all past information, thereby preserving global semantics. As illustrated in Fig. 2, the architecture follows the spirit of MAR [19], comprising a DiT-based context encoder and a lightweight MLP velocity predictor. The former encodes historical motion and text semantics and supplies them as partial conditions to the MLP predictor.

During training, we concatenate actor and reactor history tokens  $(a_i, b_i)$  along the last dimension and prepend a learnable start-of-sequence token  $\langle \text{sos} \rangle$  to ensure that inference remains feasible at  $t=0$ . The concatenated sequence is fed into the DiT backbone, while text conditioning is injected through normalization layers (via infusion), and a causal mask is applied to enforce forward-only temporal dependencies for autoregressive learning. The encoded historical context  $c_i$  is then combined with the upsampled timesteps  $(r, t)$  and used as conditions for an AdaLN-modulated MLP. At the current step, the interpolated reactor sample  $b_i^{r,t}$  from the velocity field is passed to the MLP velocity predictor, which outputs the average velocity  $\hat{u}_{r,t}$ . Unlike offline generation, the conditioning input here includes not only the current actor but also the accumulated history; consequently, when performing classifier-free guidance (CFG), we augment the null token with a *null history* to match the online conditioning interface.

At inference time, the start token  $\langle \text{sos} \rangle$  is first encoded as the initial history. A Gaussian noise token  $\epsilon_1$  is then paired with the current actor token  $a_1$  and fed into the MLP with  $(r=0, t=1)$  to predict the average velocity  $\hat{u}_1$ . The current reactor token is obtained by  $b_1 = \epsilon_1 - \hat{u}_1$  according to Eq.4. The predicted reactor token is cached together with the corresponding actor token to update the history, and the process is iterated autoregressively until actor tokens end.

### 4.4. Bootstrap Contextual Encoding

Drift over long sequences is an inherent limitation of autoregressive models. HumanX [16] addresses this through a history-rollout training strategy, where the ground-truth (GT) history condition is gradually replaced by the model’s generated history. However, this approach has three main drawbacks. First, to stabilize training, HumanX gradually subtracts the GT history from the generated ones, slow-

---

#### Algorithm 1 Bootstrap Contextual Encoding (BSCE)

---

```

1: procedure BSCE( $G_\theta, \mathcal{Y}, \mathcal{X}, \mathcal{C}, \mathcal{S}_t, K_{\max}, I_{\max}$ )
2:    $K \leftarrow 1$ 
3:   for iteration = 1 to  $I_{\max}$  do
4:     Sample  $(x_a, x_b, c)$  from  $\mathcal{Y}, \mathcal{X}, \mathcal{C}$ 
5:     Initialize context buffer  $\mathcal{Z} \leftarrow \{\langle \text{sos} \rangle\}$ 
6:      $(\{a_i\}, \{b_i^{\text{gt}}\}) \leftarrow \text{TOKENIZE}(x_a, x_b)$ 
7:     for  $i = 1$  to  $K$  do
8:        $c_i \leftarrow \text{ENCODECONTEXT}(\mathcal{Z}, c)$ 
9:       Sample  $(r, t) \sim \mathcal{S}_t, \epsilon_i \sim \mathcal{N}(0, I)$ 
10:       $\hat{u}_{r,t} \leftarrow G_\theta(\epsilon_i, a_i \text{ or } b_i, r, t, c_i)$ 
11:       $a_i \text{ or } b_i \leftarrow \epsilon_i - \hat{u}_{r,t}$ 
12:      Append  $(a_i, b_i)$  to  $\mathcal{Z}$ 
13:       $\mathcal{L}_i \leftarrow \text{LOSS}(\hat{u}_{r,t})$ 
14:    end for
15:    Update  $\theta \leftarrow \theta - \eta \nabla_\theta \left( \frac{1}{K} \sum_i \mathcal{L}_i \right)$ 
16:     $K \leftarrow \text{SCHEDULED}(\text{iteration}, K_{\max})$ 
17:  end for
18: end procedure

```

---

ing the convergence. Second, as the model converges, the generated history becomes increasingly similar to the GT, leading to insufficient self-augmentation. Third, HumanX only replaces the reactor history while keeping the actor unchanged, which lead to overfitting to the actor’s motion.

To address these limitations, we propose Bootstrap Contextual Encoding (BSCE). As detailed in Algorithm 1, BSCE replaces both actor and reactor histories with generated samples from the very beginning of training. As the model progressively aligns its outputs with the GT, the number of autoregressive iterations is gradually increased on schedule. This amplified accumulated error introduces additional noise, which in turn enhances the model’s robustness and generalization. Moreover, since HumanX relies on a multi-step diffusion model, its rollout is computationally expensive during the training phase. In contrast, our MeanFlow-based generator performs single-step inference, providing substantial efficiency gains and further highlighting BSCE’s natural compatibility with MeanFlow.

## 5. Experiments

**Datasets.** We evaluate our approach on two widely adopted benchmarks for text-conditioned human interaction synthesis: *InterHuman* [20] and *InterX* [41]. *InterHuman* comprises 7,779 interaction sequences, while *InterX* provides 11,388 sequences, each annotated with 3 textual descriptions. Compared with the other noisy and small datasets like NTU-120 and CHI3D[6, 22], these two datasets are of better motion qualities and have solid and public metrics for evaluations for fair comparisons.

The *InterHuman* dataset is built upon the AMASS [25] skeleton, which includes 22 joints with the root joint. Each

Table 2. Comparison of online methods on InterHuman and InterX datasets.

| Dataset    | Model           | FID $\downarrow$ | R-Prec@1 $\uparrow$ | R-Prec@2 $\uparrow$ | R-Prec@3 $\uparrow$ | MM Dist $\downarrow$ | Diversity $\rightarrow$ | MModality $\uparrow$ |
|------------|-----------------|------------------|---------------------|---------------------|---------------------|----------------------|-------------------------|----------------------|
| InterHuman | Ground Truth    | 0.273 $\pm$ .007 | 0.452 $\pm$ .008    | 0.610 $\pm$ .009    | 0.701 $\pm$ .008    | 3.755 $\pm$ .008     | 7.948 $\pm$ .064        | -                    |
|            | InterFormer [4] | 4.871 $\pm$ .049 | 0.302 $\pm$ .004    | 0.457 $\pm$ .004    | 0.542 $\pm$ .005    | 3.845 $\pm$ .001     | 7.482 $\pm$ .045        | 0.254 $\pm$ .029     |
|            | CAMDM [2]       | 4.000 $\pm$ .046 | 0.335 $\pm$ .005    | 0.492 $\pm$ .005    | 0.587 $\pm$ .005    | 3.828 $\pm$ .001     | 7.547 $\pm$ .025        | 1.581 $\pm$ .026     |
|            | ReGenNet [42]   | 4.176 $\pm$ .085 | 0.355 $\pm$ .005    | 0.508 $\pm$ .005    | 0.600 $\pm$ .004    | 3.817 $\pm$ .001     | 7.480 $\pm$ .033        | 0.442 $\pm$ .012     |
|            | ARMFlow (Ours)  | 2.178 $\pm$ .054 | 0.441 $\pm$ .005    | 0.605 $\pm$ .005    | 0.699 $\pm$ .005    | 3.783 $\pm$ .002     | 7.745 $\pm$ .024        | 0.369 $\pm$ .008     |
| InterX     | Ground Truth    | 0.002 $\pm$ .000 | 0.435 $\pm$ .005    | 0.628 $\pm$ .004    | 0.736 $\pm$ .004    | 3.574 $\pm$ .013     | 8.947 $\pm$ .078        | -                    |
|            | InterFormer [4] | 0.304 $\pm$ .009 | 0.301 $\pm$ .003    | 0.469 $\pm$ .003    | 0.571 $\pm$ .002    | 4.604 $\pm$ .009     | 8.579 $\pm$ .061        | 0.289 $\pm$ .009     |
|            | CAMDM [2]       | 0.429 $\pm$ .011 | 0.312 $\pm$ .004    | 0.480 $\pm$ .003    | 0.587 $\pm$ .003    | 4.468 $\pm$ .020     | 8.467 $\pm$ .072        | 1.460 $\pm$ .027     |
|            | ReGenNet [42]   | 0.071 $\pm$ .003 | 0.402 $\pm$ .005    | 0.584 $\pm$ .004    | 0.690 $\pm$ .004    | 3.843 $\pm$ .011     | 9.011 $\pm$ .053        | 0.738 $\pm$ .021     |
|            | ARMFlow (Ours)  | 0.042 $\pm$ .003 | 0.420 $\pm$ .004    | 0.606 $\pm$ .004    | 0.711 $\pm$ .004    | 3.728 $\pm$ .012     | 8.939 $\pm$ .071        | 1.203 $\pm$ .029     |

joint is represented following the HumanML3D [10] convention as  $\{\mathbf{p}_g, \mathbf{v}_g, \mathbf{r}_{6d}\}$ , where  $\mathbf{p}_g \in \mathbb{R}^3$  denotes global position,  $\mathbf{v}_g \in \mathbb{R}^3$  global velocity, and  $\mathbf{r}_{6d} \in \mathbb{R}^6$  the local 6D rotation. This results in a motion tensor  $\mathbf{m}_p \in \mathbb{R}^{N \times 22 \times 12}$ , accompanied by a binary foot-contact indicator  $fc \in \mathbb{R}^2$ .

In contrast, *InterX* adopts the SMPL-X [26] skeleton, which has 55 articulated joints covering the body, hands, and facial regions, along with the root orientation. Each joint rotation and root orientation is encoded as  $\mathbf{r}_{6d}$ , while the root translation and rotation are represented by  $\mathbf{t}_r$  and  $\mathbf{r}_r$ , respectively, forming  $\mathbf{m}_p \in \mathbb{R}^{N \times 56 \times 6}$ .

**Evaluation Metrics.** For reaction generation, we mainly focus on fidelity and semantic correspondence. To comprehensively evaluate the performance of our model, we adopt a suite of feature-space metrics by Liang et al. [20]. To assess the realism and fidelity of generated interactions, we compute the Fréchet Inception Distance (FID) and between the feature distributions of generated and ground-truth motions and their Diversity. To evaluate the semantic alignment between text prompts and generated motions, we use R-Precision and Multimodal Distance (MMDist), which measure the consistency between text input and generated motions. To assess generative quality beyond accuracy, we report Multimodality, quantifying the model’s ability to produce multiple plausible motions for the same text prompts.

**Baselines.** We divide our evaluation into two parts. For offline generation, we compare our approach with several state-of-the-art methods, including In2IN, which first synthesizes actor-reactor motions with an MDM prior and subsequently refines them; ReGenNet, a diffusion model with a transformer-decoder backbone; InterMask, a discrete autoregressive model based on masking; and an extended variant of MLD that performs diffusion in a latent space. For online generation, we benchmark against InterFormer, a conventional transformer-based autoregressive architecture; the online configuration of ReGenNet; and CAMDM, which adopts a transformer encoder and conditions on a fixed-length context window. Notably, these online base-

lines are not explicitly designed for real-time synthesis. Although ReGenNet can apply causal masking, its decoder architecture only conditions on the actor’s previous frame and cannot exploit the reactor’s past states, which often leads to temporal discontinuities. CAMDM, on the other hand, relies on a short fixed window of 10 frames, limiting long-range contextual modeling and causing pronounced drift in extended sequences, particularly on InterHuman. Furthermore, these designs do not support generation from scratch, rendering inference at  $t=0$  infeasible. In contrast, our method operates at a finer 4-frame granularity for real-time synthesis, scales more favorably than CAMDM, and does not depend on any initial motion. To ensure a fair comparison, we provide CAMDM with additional support by supplying an initial motion sequence, which compensates for its inability to generate from scratch, while keeping its 10-frame context window as specified by the authors.

**Implementation Details.** For the CNN encoder, we adopt the same design across both datasets except for the input dimension. Specifically, we follow the T2M-GPT configuration with a hidden size of 256, two residual convolutional downsampling blocks, and three hidden layers per block. For the main model, we use a standard DiT architecture as the backbone for both ARMFlow (online) and ReMFlow (offline), consisting of 512 hidden dimensions, 7 transformer layers, and 8 attention heads with skip connections. The MLP-based velocity predictor in ARMFlow is implemented as a lightweight 5-layer network, and we keep the network configuration identical across datasets. For MeanFlow, we sample timesteps from a logit-normal distribution and set the probability of instantaneous velocity sampling ( $r = t$ ) to 0.25. In ReMFlow, classifier-free guidance (CFG) strength is set to  $\omega = 1.8$  for InterHuman and  $\omega = 2.0$  for InterX. For ARMFlow, we use  $\omega = 1.8$  on InterHuman and  $\omega = 1.2$  on InterX. All models are trained with a batch size of 64. For the CNN-VAE, we train for 2000 epochs on InterHuman and 800 epochs on InterX. ReMFlow is trained for 800 epochs on InterHuman and 500 epochs on InterX, while ARMFlow converges

Table 3. Comparison of offline methods on InterHuman and InterX datasets.

| Dataset    | Model          | FID $\downarrow$        | R-Prec@1 $\uparrow$     | R-Prec@2 $\uparrow$     | R-Prec@3 $\uparrow$     | MM Dist $\downarrow$    | Diversity $\rightarrow$ | MModality $\uparrow$    |
|------------|----------------|-------------------------|-------------------------|-------------------------|-------------------------|-------------------------|-------------------------|-------------------------|
| InterHuman | Ground Truth   | 0.273 $\pm$ .007        | 0.452 $\pm$ .008        | 0.610 $\pm$ .009        | 0.701 $\pm$ .008        | 3.755 $\pm$ .008        | 7.948 $\pm$ .064        | -                       |
|            | InterGen [20]  | 9.183 $\pm$ .174        | 0.325 $\pm$ .004        | 0.467 $\pm$ .004        | 0.546 $\pm$ .005        | 3.859 $\pm$ .001        | 7.305 $\pm$ .047        | 1.270 $\pm$ .023        |
|            | in2IN [31]     | 7.913 $\pm$ .251        | 0.362 $\pm$ .004        | 0.504 $\pm$ .008        | 0.589 $\pm$ .007        | 3.832 $\pm$ .002        | 7.709 $\pm$ .040        | 1.165 $\pm$ .034        |
|            | MLD* [3]       | 3.588 $\pm$ .076        | 0.405 $\pm$ .005        | 0.561 $\pm$ .007        | 0.649 $\pm$ .006        | 3.798 $\pm$ .002        | 7.663 $\pm$ .040        | 1.124 $\pm$ .048        |
|            | ReGenNet* [42] | 2.930 $\pm$ .052        | 0.362 $\pm$ .005        | 0.513 $\pm$ .005        | 0.605 $\pm$ .004        | 3.815 $\pm$ .001        | 7.582 $\pm$ .064        | <b>1.737</b> $\pm$ .020 |
|            | InterMask [15] | 3.453 $\pm$ .061        | 0.451 $\pm$ .007        | 0.610 $\pm$ .006        | 0.701 $\pm$ .005        | 3.782 $\pm$ .002        | 7.710 $\pm$ .046        | 1.361 $\pm$ .032        |
| InterX     | ReMflow (Ours) | <b>2.433</b> $\pm$ .042 | <b>0.452</b> $\pm$ .006 | <b>0.618</b> $\pm$ .005 | <b>0.708</b> $\pm$ .005 | <b>3.778</b> $\pm$ .001 | <b>7.714</b> $\pm$ .029 | 0.685 $\pm$ .018        |
|            | Ground Truth   | 0.002 $\pm$ .000        | 0.435 $\pm$ .005        | 0.628 $\pm$ .004        | 0.736 $\pm$ .004        | 3.574 $\pm$ .013        | 8.947 $\pm$ .078        | -                       |
|            | InterGen [20]  | 0.238 $\pm$ .038        | 0.352 $\pm$ .004        | 0.542 $\pm$ .005        | 0.643 $\pm$ .004        | 4.212 $\pm$ .029        | 8.773 $\pm$ .067        | 1.552 $\pm$ .029        |
|            | MLD* [3]       | 0.148 $\pm$ .020        | 0.414 $\pm$ .004        | 0.607 $\pm$ .006        | 0.712 $\pm$ .004        | 3.655 $\pm$ .020        | 8.893 $\pm$ .053        | <b>1.875</b> $\pm$ .088 |
|            | ReGenNet [42]  | 0.093 $\pm$ .022        | 0.407 $\pm$ .004        | 0.589 $\pm$ .004        | 0.705 $\pm$ .003        | 3.762 $\pm$ .015        | 8.841 $\pm$ .072        | <b>1.937</b> $\pm$ .069 |
|            | InterMask [15] | 0.399 $\pm$ .013        | 0.429 $\pm$ .005        | 0.622 $\pm$ .005        | 0.731 $\pm$ .005        | 3.584 $\pm$ .017        | 8.911 $\pm$ .057        | 0.859 $\pm$ .033        |
|            | ReMflow (Ours) | <b>0.058</b> $\pm$ .005 | <b>0.440</b> $\pm$ .004 | <b>0.636</b> $\pm$ .004 | <b>0.743</b> $\pm$ .003 | <b>3.570</b> $\pm$ .013 | <b>8.948</b> $\pm$ .068 | 1.607 $\pm$ .039        |

faster, requiring 500 epochs and 300 epochs, respectively. All experiments use AdamW optimizer with a learning rate of  $1 \times 10^{-4}$ . All training and inference are conducted on NVIDIA H100 GPUs in an HPC environment.

## 5.1. Quantative Results

**Online Generation.** We first focus on the more challenging online generation setting. Tab. 2 reports the comparison between our ARMFlow and existing online generation models, ReGenNet and CAMDM. On the long-sequence InterHuman dataset, both baselines fail to produce satisfactory results. The primary limitation of CAMDM lies in its short context window, which prevents it from encoding the entire historical information, leading to severe temporal drift in the generated motions. Although ReGenNet utilizes the full actor history, its design initializes the reactor input from pure Gaussian noise at every inference step, making it unable to adaptively refine the reactor’s representation based on its own history, thus resulting in temporally inconsistent actions. In contrast, ARMFlow significantly outperforms existing methods in both FID and semantic consistency. Compared with CAMDM (the second-best method in FID), ARMFlow achieves a 45% relative improvement; and compared with ReGenNet (the second-best in semantic consistency), our model attains a 24.2% relative gain in R-precision (top-1). Moreover, on the shorter-sequence InterX dataset, our approach also achieves state-of-the-art results. ReGenNet performs relatively well on this dataset, which we attribute to its short-term attention mechanism being more effective when motion sequences are shorter. It is worth noting that online generation does not necessarily lead to performance degradation—in our experiments, ARMFlow even yields a lower (better) FID in the online setting than in the offline one, while the offline version, benefiting from full actor-conditioned information, achieves slightly higher semantic consistency.

**Offline Generation.** For the offline generation task, we further evaluate the generality of our ReMFlow and compare it with the current SOTA approaches in Tab. 3. InterMask, which is based on discrete random masking, performs well in semantic-matching metrics such as R-precision and MM-Distance, but its FID is considerably worse. This degradation mainly stems from its shared VQ-VAE encoder, which over-compresses motion features and thereby harms reconstruction quality—one of the key reasons we avoid discrete representations. ReGenNet, operating directly on raw data without compression, avoids such information loss; however, in the long-sequence InterHuman dataset, its self-attention mechanism struggles to capture fine-grained semantics, leading to weaker semantic consistency despite a good FID score. MLD lies between these two extremes, further validating a general trend in motion generation: stronger compression improves semantic alignment but often sacrifices reconstruction fidelity.

Notably, InterMask achieves its high semantic consistency at the cost of efficiency—it requires at least 20 inference steps, resulting in a total inference time of 0.77 s. In contrast, ReMFlow reaches state-of-the-art performance with a single forward pass, substantially improving inference speed while maintaining generation quality. Similar observations hold on the InterX dataset, where the shorter motion sequences allow ReGenNet to achieve relatively good semantic alignment as well.

## 5.2. Qualitative Comparison

We present online generation results qualitatively on the InterHuman dataset, which has longer sequences, and the competition is more challenging. We compare our method with ReGenNet, and visualize the results in Fig. 3, which indicate that our approach not only achieves better inter-person contact quality but also demonstrates stronger semantic alignment with the text prompts.

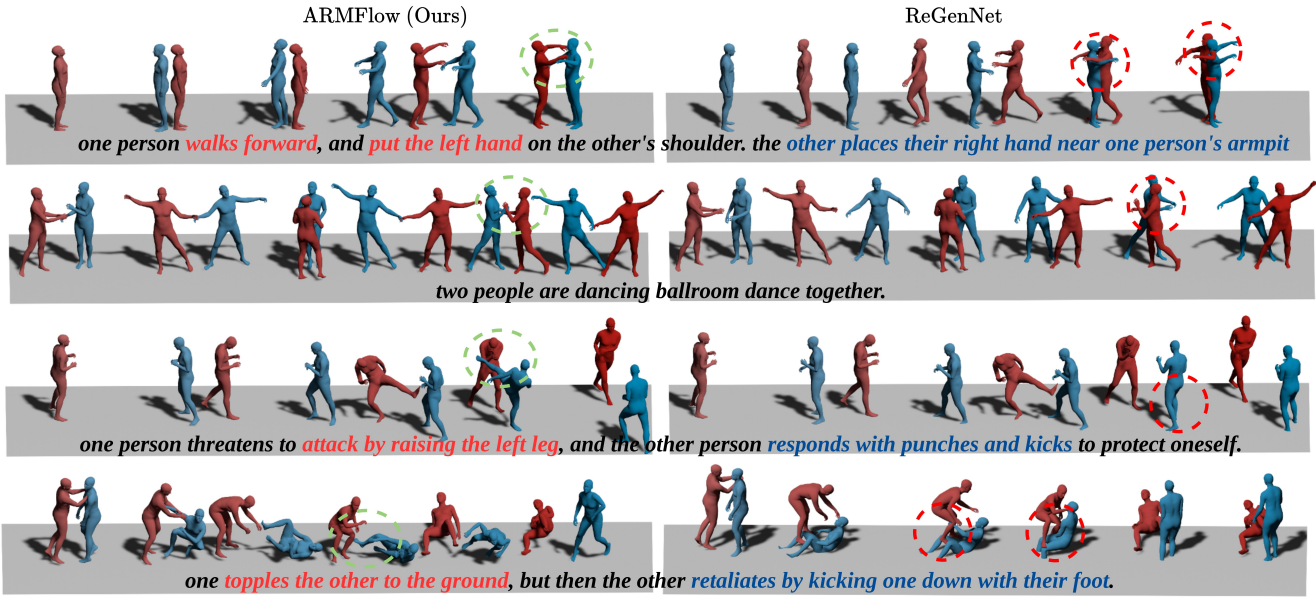


Figure 3. Qualitative comparison with ReGenNet on InterHuman dataset. The problematic interactions are marked with red dashed lines, including penetrations and semantic misalignment, and the correct ones are marked with green.

### 5.3. Ablation Study

We validate the effectiveness of our proposed designs and individual modules. First, for the generative approaches, we kept the same network architecture while replacing the objective function with Diffusion Models and Rectified Flow, respectively, and performed task-specific parameter tuning for them including CFG strength. Experimental results in Tab. 4 and Tab. 5 show that MeanFlow consistently achieves the best FID scores and semantic alignment across both online and offline generation tasks, as well as on both datasets. Moreover, its single-step generation greatly accelerates the training process when integrated with BSCE, demonstrating the broad adaptability of MeanFlow to various generation tasks. Furthermore, we compare BSCE with two alternative strategies: using ground-truth contextual encoding (GTE) and progressive rollout. BSCE significantly outperforms both approaches, confirming the effectiveness and superiority of our proposed method.

Table 4. Ablation study for online generation on methods.

| Model      | R-Prec@3 ↑        | FID ↓                         | MM Dist ↓                     | Diversity →                                                 |
|------------|-------------------|-------------------------------|-------------------------------|-------------------------------------------------------------|
| InterHuman | DDIM 10           | 0.689 <sup>±.004</sup>        | 3.528 <sup>±.049</sup>        | 3.803 <sup>±.002</sup> 7.691 <sup>±.037</sup>               |
|            | DDIM 50           | 0.697 <sup>±.005</sup>        | 3.449 <sup>±.062</sup>        | 3.794 <sup>±.002</sup> 7.702 <sup>±.028</sup>               |
|            | DDPM              | 0.686 <sup>±.004</sup>        | 3.757 <sup>±.068</sup>        | 3.806 <sup>±.002</sup> <b>7.803</b> <sup>±.035</sup>        |
|            | Rectified Flow 10 | 0.692 <sup>±.004</sup>        | <u>2.449</u> <sup>±.062</sup> | 3.796 <sup>±.001</sup> 7.702 <sup>±.028</sup>               |
|            | ARMFlow (Ours)    | <b>0.699</b> <sup>±.005</sup> | <b>2.178</b> <sup>±.054</sup> | <b>3.783</b> <sup>±.002</sup> 7.745 <sup>±.024</sup>        |
| InterX     | DDIM 10           | 0.692 <sup>±.004</sup>        | 0.093 <sup>±.005</sup>        | 3.802 <sup>±.014</sup> 8.870 <sup>±.066</sup>               |
|            | DDIM 50           | 0.705 <sup>±.004</sup>        | 0.064 <sup>±.004</sup>        | <u>3.733</u> <sup>±.013</sup> 8.895 <sup>±.062</sup>        |
|            | DDPM              | 0.695 <sup>±.004</sup>        | 0.106 <sup>±.006</sup>        | 3.792 <sup>±.015</sup> <u>8.920</u> <sup>±.088</sup>        |
|            | Rectified Flow 10 | 0.698 <sup>±.005</sup>        | 0.059 <sup>±.004</sup>        | 3.784 <sup>±.011</sup> 8.913 <sup>±.072</sup>               |
|            | ARMFlow (Ours)    | <b>0.711</b> <sup>±.004</sup> | <b>0.042</b> <sup>±.003</sup> | <b>3.728</b> <sup>±.012</sup> <b>8.939</b> <sup>±.071</sup> |

Table 5. Ablation study for offline generation on methods.

| Model      | R-Prec@3 ↑        | FID ↓                         | MM Dist ↓                     | Diversity →                                                 |
|------------|-------------------|-------------------------------|-------------------------------|-------------------------------------------------------------|
| InterHuman | DDIM 10           | 0.677 <sup>±.006</sup>        | 3.931 <sup>±.050</sup>        | 3.800 <sup>±.002</sup> 7.622 <sup>±.025</sup>               |
|            | DDIM 50           | <u>0.694</u> <sup>±.004</sup> | 2.918 <sup>±.068</sup>        | <u>3.789</u> <sup>±.003</sup> 7.656 <sup>±.040</sup>        |
|            | DDPM              | 0.681 <sup>±.005</sup>        | 3.595 <sup>±.051</sup>        | 3.797 <sup>±.002</sup> 7.663 <sup>±.035</sup>               |
|            | Rectified Flow 10 | 0.678 <sup>±.005</sup>        | <u>2.906</u> <sup>±.044</sup> | 3.801 <sup>±.002</sup> <b>7.775</b> <sup>±.045</sup>        |
|            | ReMFlow(Ours)     | <b>0.708</b> <sup>±.005</sup> | <b>2.433</b> <sup>±.042</sup> | <b>3.778</b> <sup>±.001</sup> <u>7.714</u> <sup>±.029</sup> |
| InterX     | DDIM 10           | 0.699 <sup>±.005</sup>        | 0.127 <sup>±.036</sup>        | 3.805 <sup>±.012</sup> 8.804 <sup>±.059</sup>               |
|            | DDIM 50           | 0.700 <sup>±.004</sup>        | <u>0.095</u> <sup>±.076</sup> | 3.749 <sup>±.013</sup> 8.842 <sup>±.077</sup>               |
|            | DDPM              | 0.671 <sup>±.005</sup>        | 3.595 <sup>±.051</sup>        | 3.893 <sup>±.012</sup> 8.857 <sup>±.063</sup>               |
|            | Rectified Flow 10 | <u>0.737</u> <sup>±.007</sup> | 0.103 <sup>±.015</sup>        | <u>3.645</u> <sup>±.012</sup> <u>8.941</u> <sup>±.087</sup> |
|            | ReMFlow(Ours)     | <b>0.743</b> <sup>±.003</sup> | <b>0.058</b> <sup>±.005</sup> | <b>3.570</b> <sup>±.013</sup> <b>8.948</b> <sup>±.068</sup> |

Table 6. Ablation on the training strategies for online autoregressive diffusion. GTE stands for ground-truth encoding, Rollout is the strategy used in HumanX[16], and BSCE is our strategy.

| Model      | R-Prec@3 ↑      | FID ↓                         | MM Dist ↓                     | Diversity →                                                 |
|------------|-----------------|-------------------------------|-------------------------------|-------------------------------------------------------------|
| InterHuman | Ground Truth    | 0.701 <sup>±.008</sup>        | 0.273 <sup>±.007</sup>        | 3.755 <sup>±.008</sup> 7.948 <sup>±.064</sup>               |
|            | ARMFlow-GTE     | 0.602 <sup>±.004</sup>        | 5.136 <sup>±.040</sup>        | 3.813 <sup>±.002</sup> 7.728 <sup>±.033</sup>               |
|            | ARMFlow-Rollout | 0.675 <sup>±.005</sup>        | 4.161 <sup>±.055</sup>        | 3.798 <sup>±.002</sup> <b>7.802</b> <sup>±.038</sup>        |
|            | ARMFlow(Ours)   | <b>0.699</b> <sup>±.005</sup> | <b>2.178</b> <sup>±.054</sup> | <b>3.783</b> <sup>±.002</sup> 7.745 <sup>±.024</sup>        |
| InterX     | Ground Truth    | 0.736 <sup>±.004</sup>        | 0.002 <sup>±.000</sup>        | 3.574 <sup>±.013</sup> 8.947 <sup>±.078</sup>               |
|            | ARMFlow-GTE     | 0.630 <sup>±.003</sup>        | 0.548 <sup>±.007</sup>        | 4.667 <sup>±.020</sup> 8.435 <sup>±.068</sup>               |
|            | ARMFlow-Rollout | 0.670 <sup>±.004</sup>        | 0.192 <sup>±.006</sup>        | 4.321 <sup>±.013</sup> 8.743 <sup>±.082</sup>               |
|            | ARMFlow(Ours)   | <b>0.711</b> <sup>±.004</sup> | <b>0.042</b> <sup>±.003</sup> | <b>3.728</b> <sup>±.012</sup> <b>8.939</b> <sup>±.071</sup> |

### 6. Conclusion

We presented ARMFlow, the first MeanFlow-based framework for real-time 3D human reaction generation, achieving single-step inference while maintaining high-fidelity and context-awareness. Our causal context encoder and Bootstrap Context Encoding (BSCE) effectively address long-term dependency modeling and autoregressive error accu-

mulation, enabling robust and efficient online generation. We also introduce ReMFlow as a versatile offline baseline, demonstrating state-of-the-art performance with unprecedented inference speed. Overall, our work establishes a scalable and practical framework for both online and offline human motion generation, paving the way for real-world applications in Human-Robot Interaction, AR, and VR.

Despite these strengths, our method has certain limitations. First, from an engineering perspective, the current implementation does not provide elastic delay handling for the autoregressive small window, which may lead to minor asynchronous behaviors when multiple agents interact. Second, due to the nature of MeanFlow, it does not support post-hoc classifier guidance like diffusion-based models, preventing the use of optimization-based corrections to further refine generated motions. Addressing these limitations represents promising directions for future work.

## References

- [1] Huiwen Chang, Han Zhang, Lu Jiang, Ce Liu, and William T. Freeman. Maskgit: Masked generative image transformer. In *The IEEE Conference on Computer Vision and Pattern Recognition (CVPR)*, 2022. [3](#)
- [2] Rui Chen, Mingyi Shi, Shaoli Huang, Ping Tan, Taku Komura, and Xuelin Chen. Taming diffusion probabilistic models for character control. In *ACM SIGGRAPH 2024 Conference Papers*, New York, NY, USA, 2024. Association for Computing Machinery. [2, 3, 6](#)
- [3] Xin Chen, Wen Jiang, Biao Liu, Zilong Huang, Bin Fu, Tao Chen, and Gang Yu. Executing your commands via motion diffusion in latent space. In *Proceedings of the IEEE/CVF Conference on Computer Vision and Pattern Recognition (CVPR)*, 2023. [1, 2, 7](#)
- [4] Baptiste Chopin, Hao Tang, Naima Otberdout, Mohamed Daoudi, and Nicu Sebe. Interaction transformer for human reaction generation. *IEEE Transactions on Multimedia (TMM)*, pages 1–13, 2023. [2, 6](#)
- [5] Christian Diller and Angela Dai. Cg-hoi: Contact-guided 3d human-object interaction generation. In *Proceedings of the IEEE/CVF Conference on Computer Vision and Pattern Recognition (CVPR)*, pages 19888–19901, 2024. [1, 2](#)
- [6] Mihai Fieraru, Mihai Zanfir, Elisabeta Oneata, Alin-Ionut Popa, Vlad Olaru, and Cristian Sminchisescu. Three-dimensional reconstruction of human interactions. In *The IEEE/CVF Conference on Computer Vision and Pattern Recognition (CVPR)*, 2020. [5](#)
- [7] Zhengyang Geng, Mingyang Deng, Xingjian Bai, J Zico Kolter, and Kaiming He. Mean flows for one-step generative modeling. *arXiv preprint arXiv:2505.13447*, 2025. [2, 3, 4](#)
- [8] Zichen Geng, Zeeshan Hayder, Wei Liu, and Ajmal Saeed Mian. Auto-regressive diffusion for generating 3d human-object interactions. In *Proceedings of the AAAI Conference on Artificial Intelligence (AAAI)*, pages 3131–3139, 2025. [1, 2](#)
- [9] Michal Geyer, Omer Bar-Tal, Shai Bagon, and Tali Dekel. Tokenflow: Consistent diffusion features for consistent video editing. In *The Twelfth International Conference on Learning Representations (ICLR)*, 2024. [3](#)
- [10] Chuan Guo, Xinxin Zuo, Sen Wang, Shihao Zou, Qingyao Sun, Annan Deng, Minglun Gong, and Li Cheng. Action2motion: Conditioned generation of 3d human motions. In *Proceedings of the 28th ACM International Conference on Multimedia (ACM MM)*, 2020. [1, 2, 6](#)
- [11] Chuan Guo, Yuxuan Mu, Muhammad Gohar Javed, Sen Wang, and Li Cheng. Momask: Generative masked modeling of 3d human motions. In *Proceedings of the IEEE/CVF Conference on Computer Vision and Pattern Recognition (CVPR)*, pages 1900–1910, 2024. [1, 2](#)
- [12] Bo Han, Hao Peng, Minjing Dong, Yi Ren, Yixuan Shen, and Chang Xu. Amd: Autoregressive motion diffusion. In *Proceedings of the AAAI Conference on Artificial Intelligence (AAAI)*, pages 2022–2030, 2024. [3](#)
- [13] Kaiming He, Xinlei Chen, Saining Xie, Yanghao Li, Piotr Dollár, and Ross Girshick. Masked autoencoders are scalable vision learners. In *Proceedings of the IEEE/CVF Conference on Computer Vision and Pattern Recognition (CVPR)*, 2022. [3](#)
- [14] Emiel Hoogeboom, Alexey A Gritsenko, Jasmijn Bastings, Ben Poole, Rianne van den Berg, and Tim Salimans. Autoregressive diffusion models. In *International Conference on Learning Representations (ICLR)*, 2022. [3](#)
- [15] Muhammad Gohar Javed, Chuan Guo, Li Cheng, and Xingyu Li. Intermask: 3d human interaction generation via collaborative masked modeling. In *The Thirteenth International Conference on Learning Representations (ICLR)*, 2025. [2, 7](#)
- [16] Kaiyang Ji, Ye Shi, Zichen Jin, Kangyi Chen, Lan Xu, Yuexin Ma, Jingyi Yu, and Jingya Wang. Towards immersive human-x interaction: A real-time framework for physically plausible motion synthesis. *arXiv preprint arXiv:2508.02106*, 2025. [2, 3, 5, 8](#)
- [17] Jiaman Li, Alexander Clegg, Roozbeh Mottaghi, Jiajun Wu, Xavier Puig, and C Karen Liu. Controllable human-object interaction synthesis. *arXiv preprint arXiv:2312.03913*, 2023. [1, 2](#)
- [18] Tianyu Li, Calvin Qiao, Guanqiao Ren, KangKang Yin, and Sehoon Ha. Aamdm: Accelerated auto-regressive motion diffusion model. In *Proceedings of the IEEE/CVF Conference on Computer Vision and Pattern Recognition (CVPR)*, pages 1813–1823, 2024. [3](#)
- [19] Tao Li, Yu Tian, Hang Li, Mingyuan Deng, and Kaiming He. Autoregressive image generation without vector quantization. In *Proceedings of the 38th Annual Conference on Neural Information Processing Systems (NeurIPS)*, 2024. To appear. [3, 5](#)
- [20] Han Liang, Wenqian Zhang, Wenxuan Li, Jingyi Yu, and Lan Xu. Intergen: Diffusion-based multi-human motion generation under complex interactions. *International Journal of Computer Vision (IJCV)*, pages 1–21, 2024. [2, 5, 6, 7](#)
- [21] Yaron Lipman, Ricky TQ Chen, Heli Ben-Hamu, Maximilian Nickel, and Matt Le. Flow matching for generative mod-

eling. In *11th International Conference on Learning Representations (ICLR)*, 2023. 3

[22] Jun Liu, Amir Shahroudy, Mauricio Perez, Gang Wang, Ling-Yu Duan, and Alex C Kot. Ntu rgb+d 120: A large-scale benchmark for 3d human activity understanding. *IEEE Transactions on Pattern Analysis and Machine Intelligence (PAMI)*, 42(10):2684–2701, 2020. 5

[23] Xingchao Liu, Chengyue Gong, et al. Flow straight and fast: Learning to generate and transfer data with rectified flow. In *The Eleventh International Conference on Learning Representations (ICLR)*, 2023. 3

[24] Zhenzhong Luo, Yuwen Xiong, Xuancheng Sun, Yang Long, Ting Yao, and Tao Mei. Learning transferable visual models from natural language supervision. In *Proceedings of the IEEE/CVF Conference on Computer Vision and Pattern Recognition (CVPR)*, 2020. 4

[25] Naureen Mahmood, Nima Ghorbani, Nikolaus F. Troje, Gerard Pons-Moll, and Michael J. Black. AMASS: Archive of motion capture as surface shapes. In *International Conference on Computer Vision (ICCV)*, pages 5442–5451, 2019. 5

[26] Georgios Pavlakos, Vasileios Choutas, Nima Ghorbani, Timo Bolkart, Ahmed A. A. Osman, Dimitrios Tzionas, and Michael J. Black. Expressive body capture: 3D hands, face, and body from a single image. In *Proceedings IEEE Conf. on Computer Vision and Pattern Recognition (CVPR)*, pages 10975–10985, 2019. 6

[27] William Peebles and Saining Xie. Scalable diffusion models with transformers. In *Proceedings of the IEEE/CVF International Conference on Computer Vision (ICCV)*, pages 4172–4182. IEEE Computer Society, 2023. 4

[28] Xiaogang Peng, Yiming Xie, Zizhao Wu, Varun Jampani, Deqing Sun, and Huaizu Jiang. Hoi-diff: Text-driven synthesis of 3d human-object interactions using diffusion models. *arXiv preprint arXiv:2312.06553*, 2023. 1, 2

[29] Mathis Petrovich, Michael J. Black, and GÜl Varol. Action-conditioned 3D human motion synthesis with transformer VAE. In *International Conference on Computer Vision (ICCV)*, 2021. 2

[30] Mathis Petrovich, Michael J. Black, and GÜl Varol. TEMOS: Generating diverse human motions from textual descriptions. In *European Conference on Computer Vision (ECCV)*, 2022. 1, 2

[31] Pablo Ruiz-Ponce, German Barquero, Cristina Palmero, Sergio Escalera, and José García-Rodríguez. in2in: Leveraging individual information to generate human interactions. In *Proceedings of the IEEE/CVF Conference on Computer Vision and Pattern Recognition (CVPR) Workshops*, pages 1941–1951, 2024. 2, 7

[32] Jiaming Song, Chenlin Meng, and Stefano Ermon. Denoising diffusion implicit models. In *International Conference on Learning Representations (ICLR)*, 2021. 2

[33] NextStep Team, Chunrui Han, Guopeng Li, Jingwei Wu, Quan Sun, Yan Cai, Yuang Peng, Zheng Ge, Deyu Zhou, Haomiao Tang, Hongyu Zhou, Kenkun Liu, Ailin Huang, Bin Wang, Changxin Miao, Deshan Sun, En Yu, Fukun Yin, Gang Yu, Hao Nie, Haoran Lv, Hanpeng Hu, Jia Wang, Jian Zhou, Jianjian Sun, Kaijun Tan, Kang An, Kangheng Lin, Liang Zhao, Mei Chen, Peng Xing, Rui Wang, Shiyu Liu, Shutao Xia, Tianhao You, Wei Ji, Xianfang Zeng, Xin Han, Xuelin Zhang, Yana Wei, Yanming Xu, Yimin Jiang, Yingming Wang, Yu Zhou, Yucheng Han, Ziyang Meng, Binxing Jiao, Daxin Jiang, Xiangyu Zhang, and Yibo Zhu. Nextstep-1: Toward autoregressive image generation with continuous tokens at scale. *arXiv preprint arXiv:2508.10711*, 2025. 3

[34] Guy Tevet, Sigal Raab, Brian Gordon, Yoni Shafir, Daniel Cohen-or, and Amit Haim Bermano. Human motion diffusion model. In *The Eleventh International Conference on Learning Representations (ICLR)*, 2023. 1, 2

[35] Keyu Tian, Yicheng Jiang, Ziyang Yuan, Bo Peng, and Lijuan Wang. Visual autoregressive modeling: Scalable image generation via next-scale prediction. In *Proceedings of the 37th Annual Conference on Neural Information Processing Systems (NeurIPS)*, pages 84839–84865, 2024. NeurIPS 2024 Best Paper. 3

[36] Ashish Vaswani, Noam Shazeer, Niki Parmar, Jakob Uszkoreit, Llion Jones, Aidan N Gomez, Łukasz Kaiser, and Illia Polosukhin. Attention is all you need. *Advances in neural information processing systems (NeurIPS)*, 30, 2017. 2

[37] Yin Wang, Zhiying Leng, Frederick WB Li, Shun-Cheng Wu, and Xiaohui Liang. Fg-t2m: Fine-grained text-driven human motion generation via diffusion model. In *Proceedings of the IEEE/CVF International Conference on Computer Vision (ICCV)*, pages 22035–22044, 2023. 1, 2

[38] Yinhui Wang, Jing Lin, Ailing Zeng, Zhengyi Luo, Jian Zhang, and Lei Zhang. Physhoi: Physics-based imitation of dynamic human-object interaction. *arXiv preprint arXiv:2312.04393*, 2023. 2

[39] Yabiao Wang, Shuo Wang, Jiangning Zhang, Ke Fan, Jiafu Wu, Zhucun Xue, and Yong Liu. Timotion: Temporal and interactive framework for efficient human-human motion generation. In *Proceedings of the Computer Vision and Pattern Recognition Conference (CVPR)*, pages 7169–7178, 2025. 2

[40] YB Wang, Shuo Wang, JN Zhang, JF Wu, QD He, CC Fu, CJ Wang, and Yong Liu. Marrs: Masked autoregressive unit-based reaction synthesis. *arXiv preprint arXiv:2505.11334*, 2025. 2

[41] Liang Xu, Xintao Lv, Yichao Yan, Xin Jin, Shuwen Wu, Congsheng Xu, Yifan Liu, Yizhou Zhou, Fengyun Rao, Xingdong Sheng, et al. Inter-x: Towards versatile human-human interaction analysis. In *CVPR*, pages 22260–22271, 2024. 1, 5

[42] Liang Xu, Yizhou Zhou, Yichao Yan, Xin Jin, Wenhan Zhu, Fengyun Rao, Xiaokang Yang, and Wenjun Zeng. Regennet: Towards human action-reaction synthesis. In *CVPR*, pages 1759–1769, 2024. 2, 6, 7

[43] Sirui Xu, Zhengyuan Li, Yu-Xiong Wang, and Liang-Yan Gui. InterDiff: Generating 3d human-object interactions with physics-informed diffusion. In *ICCV*, 2023. 1, 2

[44] Lijun Yu, José Lezama, Nitesh Bharadwaj Gundavarapu, Luca Versari, Kihyuk Sohn, David Minnen, Yong Cheng, Agrim Gupta, Xiuye Gu, Alex Hauptmann, Boqing Gong, Ming-Hsuan Yang, Irfan Essa, David Ross, and Lu Jiang. Language model beats diffusion – tokenizer is key to visual generation. In *ICLR*, 2024. 3

- [45] Jianrong Zhang, Yangsong Zhang, Xiaodong Cun, Shaoli Huang, Yong Zhang, Hongwei Zhao, Hongtao Lu, and Xi Shen. T2m-gpt: Generating human motion from textual descriptions with discrete representations. In *Proceedings of the IEEE/CVF Conference on Computer Vision and Pattern Recognition (CVPR)*, 2023. [1](#), [2](#), [3](#), [4](#)
- [46] Mingyuan Zhang, Zhongang Cai, Liang Pan, Fangzhou Hong, Xinying Guo, Lei Yang, and Ziwei Liu. Motiondiffuse: Text-driven human motion generation with diffusion model. *IEEE Transactions on Pattern Analysis and Machine Intelligence (PAMI)*, 2024.
- [47] Chongyang Zhong, Lei Hu, Zihao Zhang, and Shihong Xia. Att2m: Text-driven human motion generation with multi-perspective attention mechanism. In *Proceedings of the IEEE/CVF International Conference on Computer Vision (ICCV)*, pages 509–519, 2023. [1](#), [2](#)